AD719428

TECHNICAL REPORT NO. 6
PROJECT A-519

INVESTIGATION OF MANMADE AND NATURAL PERTURBATIONS OF THE EARTH'S ELECTRIC FIELD

C. H. Bonham III
and
J. B. Langley

Department of the Navy
Office of Naval Research
Contract Nonr-991(08)

30 October 1970

Engineering Experiment Station
GEORGIA INSTITUTE OF TECHNOLOGY
Atlanta, Georgia

DISTRIBUTION STATEMENT A
Approved for public release;
Distribution Unlimited

D D C
RECEIVED
MAR 3 1971
C

Reproduced by
NATIONAL TECHNICAL
INFORMATION SERVICE
Springfield, Va. 22151

Engineering Experiment Station
GEORGIA INSTITUTE OF TECHNOLOGY
Atlanta, Georgia

Technical Report No. 6
Project No. A-519

INVESTIGATION OF MANMADE AND NATURAL PERTURBATIONS OF THE EARTH'S ELECTRIC FIELD

By

C. H. Bonham III and J. B. Langley

30 October 1970

D D C
RECEIVED
MAR 9 1971
C

U. S. Navy Department
Office of Naval Research
Contract Nonr-991(08)

ABSTRACT

This report describes an investigation of the effect of low frequency periodic perturbations of the height of a conducting surface on the earth's local electric field.

Simulation of small, low audio frequency vibrations of a portion of a conducting surface indicates that such displacement will result in perturbations to the normal component of the electric field above that surface. The exact magnitude of these perturbations is a function of the type of probe used to sense the perturbations and the probe-to-surface distance and is, in general, on the order of microvolts.

Atmospheric noise spectra were obtained by use of a passive antenna measurement scheme. The data obtained were analyzed using the Fast Fourier Transform and noise spectra on the band 0.1 to 100 Hertz were acquired. The noise spectra thus obtained indicate that atmospheric noise appears to fall off at the rate of 27 dB per decade in the region 0.1 to 100 Hertz.

Examination of the signal-to-noise ratios implies that the performance of this system in detection of sea surface vibrations would be marginal at best.

TABLE OF CONTENTS

		Page
I.	INTRODUCTION	1
II.	SIGNAL ESTIMATES	3
III.	NOISE ESTIMATES	16
IV.	ANALYSIS AND CONCLUSIONS	34
V.	REFERENCES	35
	APPENDICES	36

LIST OF FIGURES

Figure		Page
1.	Suspended Probe Model	6
2.	Equivalent Circuit of Probe	8
3.	Probe Response as Function of Displacement, δ, for Given Values of Initial Capacitance (picofarads)	11
4.	Probe Response as Function of Initial Capacitance for Given Values of Displacement	12
5.	Geometry for Small Perturbation below Probe	14
6.	Expanded Probe Model	18
7.	Pictorial Diagram of Experiment	23
8.	Electrometer Feedback Circuit	24
9.	Atmospheric Potential Fluctuations as Measured by 1 Meter Diameter Probe 15 cm above Ground Plane -- Fair Weather	26
10.	Atmospheric Potential Fluctuations as Measured by 1 Meter Diameter Probe 15 cm above Ground Plane -- Thunderstorm Activity	27
11.	Atmospheric Noise Spectrum from 0.1 to 100 Hertz	31
12.	System Noise Spectrum from 0.1 to 100 Hertz	32

I. INTRODUCTION

In the past, work on Contract Nonr-991(08) has been directed toward various techniques for sensing underwater acoustic signals from a platform entirely removed from the surface of the sea. The early phases of the work were concerned with detecting the perturbations, caused by acoustic energy, to the permittivity of the sea water. In the later years of the research, work was directed towards a technique to detect small scale vibrations of the sea surface, again caused by acoustic energy propagating beneath the surface.

In this phase of Contract Nonr-991(08), research has been conducted to investigate the detectability of manmade free water surface motion by sensing means of perturbations to the normal component of the earth's atmospheric electric field.

The research work has been conducted with two objectives in mind: first, to provide a model for the sea surface motion in order to estimate the magnitude of the signal one could expect to detect, and second, to characterize spectrally the random variations in the earth's atmospheric electric field which would appear as background noise in the detection equipment. These data are then used to estimate a signal-to-noise ratio that characterizes the detection process.

Since the types of acoustic activity for which detection is desired are expected to induce sea surface vibrations with frequencies generally less than 100 Hertz, the noise spectra were measured in the range of 0.1 to 100 Hertz.

Section II of this report discusses the estimation of vibration-induced signals and a typical detection scheme. Section III describes the noise characterization technique, while Section IV analyzes the results of measurement of atmospheric electric field fluctuations. The Appendices describe specific features of the data collection and analysis procedures.

II. SIGNAL ESTIMATES

A. Background

When dealing with electrostatic boundary-value problems, certain conditions must be satisfied. Some of these conditions are:

(1) Laplace's equation for the potential, V, must equal zero everywhere except on boundaries.

(2) The tangential component of the electric field, E_t, must be continuous across the boundary.

(3) The normal component of the electric flux density, D_n, must be discontinuous by the amount of surface charge density at the boundary.

If we have a conducting surface with a periodic perturbation on it described by

$$Z_o = \zeta_o \cos \beta X$$

and static electric field

$$\bar{E} = E_o \hat{a}_z \quad ,$$

condition (2) requires that the field be perpendicular to the surface. Solving Laplace's equation for the potential

$$\frac{\partial^2 V}{\partial X^2} + \frac{\partial^2 V}{\partial Z^2} = 0$$

subject to the boundary conditions:

$$V = 0 \quad \text{when } Z = Z_o = \zeta_o \cos \beta X$$

$$V = E_o Z \text{ when } Z \to \infty \quad ,$$

we find the solution

$$V = E_o(Z - \zeta_o e^{\zeta\beta} \cos \beta X \; e^{-\beta Z} \cos \beta X)$$

where $\beta = 2\pi/\lambda$.

When $\beta\zeta \ll 1$, this expression can be simplified to

$$V \simeq E_o(Z - \zeta_o e^{-\beta Z} \cos \beta X)$$

Then

$$\bar{E} = -\frac{\partial V}{\partial X}\bar{a}_x - \frac{\partial V}{\partial Z}\bar{a}_y$$

$$= -(E_o \beta \zeta_o e^{-\beta Z} \sin \beta X)\,\bar{a}_x - E_o(1 - \zeta_o \beta e^{-\beta Z} \cos \beta X)\bar{a}_z$$

Both the electric field and the potential are disturbed in the same manner as the surface. The effect of the surface disturbance falls off exponentially as we move up from the surface. Therefore, either field measurements or potential measurements made near the surface will show the surface perturbation. Of these two measurements, the potential measurement is the easiest to make because it is a point measurement, while the E field is a difference or gradient measurement.

One way that these measurements can be made is to suspend a sphere or a conductor of any other practical shape above the surface. If, in the absence of the sphere, the potential of this point is V, then when the

sphere is grounded in this position, the conductor must transfer a charge of such value as to make the potential zero. If proper instrumentation is placed in the ground-to-probe path, the charge can be measured and the potential determined. If the change in potential due to the surface perturbation is all that is desired, then the distortion of the field caused by the probe will not have to be accounted for.

This type of measurement can also be used to measure surface displacements whose periods are shorter than the relaxation time for electrical phenomena in the atmosphere. This relaxation time is defined as the time it takes to transfer charge to or from a conductor by ionic conduction. Since actual values of the relaxation time for air near the earth's surface are from 5 to 40 minutes depending on the amount of pollution,[1] the case of primary interest in this study is the one in which the period of the displacement is shorter than the relaxation time. In this case, the problem is dealt with in terms of electrostatic effects rather than current effects and the change of potential between the probe and ground is related to the change of the probe-ground capacitance.

A model of the probe suspended above a conducting plane is shown in Figure 1. In this figure the capacitor is the probe-ground capacitance, the resistor is the resistance of the air column between the ground and the probe, and the current source represents the conduction current that flows in the air. This model is valid for the two conditions mentioned above. If a perturbation causes the probe-to-ground distance to change slowly as compared to the RC time constant, then the capacitive reactance is large compared to the resistance and the voltage from the probe-to-ground is just

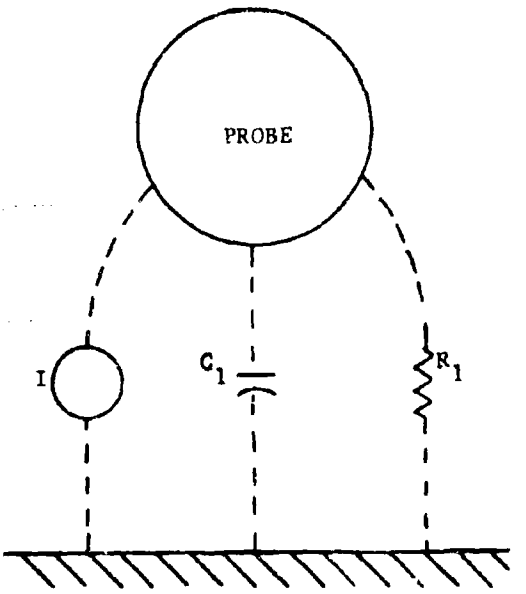

Figure 1. Suspended Probe Model

the potential of that point in space. However, if the perturbation causes the probe-to-ground distance to change rapidly with respect to the time constant, the capacitive reactance is small compared to the resistance, the probe-voltage remains constant and we have a electrostatic problem.

B. Simulation Model

In order to estimate the magnitude of the field disturbances caused by surface height perturbations, a simulation model of the proposed system was devised. The model shown in Figure 1, enlarged to include a few more variables, was used for this purpose. A schematic diagram of this circuit is shown in Figure 2. This circuit uses a Thevenin equivalent voltage source in place of the current source shown in Figure 1, and the capacitance, C_2, and resistance, R_2, represent the input impedance of the measurement instrumentation and the stray capacitance of the leads. Since we are primarily interested in events that occur faster than the relaxation time, the potential at the probe is shown as a battery.

Let V_1 be the voltage across R_1 and V_2 be the voltage across C_1, C_2 and R_2. Then solving for V_2, we know that

$$i_0 = i_1 + i_2 + i_3 \tag{1}$$

where $i_1 = \frac{dq_1}{dt}$, $i_2 = \frac{dq_2}{dt}$, $i_3 = \frac{V_2}{R_2}$,

$q_1 = C_1V_2$, and $q_2 = C_2V_2$.

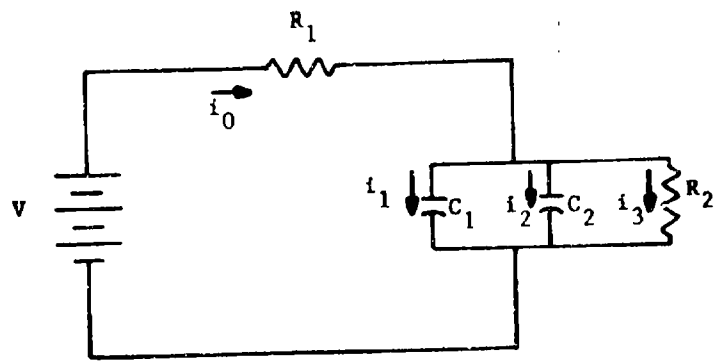

Figure 2. Equivalent Circuit of Probe

If the surface below the probe is perturbed in some periodic manner, the probe-to-ground capacitance will change proportionately due to the change in spacing. Since C_1 and V_2 are both functions of time,

$$\frac{dq_1}{dt} = C_1 \frac{dV_2}{dt} + V_2 \frac{dC_1}{dt} \tag{2}$$

$$\frac{dq_2}{dt} = C_2 \frac{dV_2}{dt} \tag{3}$$

Substituting equations (2) and (3) into equation (1) yields

$$i_0 = C_1 \frac{dV_2}{dt} + V_2 \frac{dC_1}{dt} + C_2 \frac{dV_2}{dt} + \frac{V_2}{R_2} \tag{4}$$

and making the substitution

$$i_0 = \frac{V_1}{R_1} = \frac{V - V_2}{R_1}$$

results in a differential equation in V_2

$$\frac{dV_2}{dt} = \frac{V}{R_1(C_1 + C_2)} - \frac{V_2}{(C_1 + C_2)} \left(\frac{dC_1}{dt} + \frac{1}{R_2} + \frac{1}{R_1} \right) \tag{5}$$

If we assume that the perturbation is sinusoidal, then because capacitance is inversely proportional to the spacing, C_1 will be of the form

$$C_1 = \frac{C_0}{1 - \delta/2 + (\delta/2)\cos \omega t} = \frac{C_0}{Z} \tag{6}$$

where C_0 is the capacitance at maximum spacing

δ is the ratio of peak-to-peak displacement to maximum plate separation, and

ω is the angular frequency of the perturbation

Equation (5) can now be rewritten

$$\frac{dV_2}{dt} = \left[\frac{V}{R_1} - \frac{1}{R_1} + \frac{1}{R_2} + \frac{\frac{\omega\delta C_0}{2} \sin \omega t}{Z^2} V_2\right]\left[\frac{Z}{C_0 + C_2 Z}\right] \tag{7}$$

C. Simulation Results

An estimate for the atmospheric potential, V, can be derived from the fact that the average fair-weather value of the earth's electric field is 100 volts per meter.[2] The capacitance, C_1, can be calculated from probe size and height figures, and R_1 can be estimated from the fact that the time constant, C_1R_1, will be in the range of 5 to 40 minutes, depending upon the amount of pollution in the air.

For a 1 meter diameter plate mounted 15 centimeters above the ground, the probe-to-ground capacitance would be approximately 50 picofarads and the potential between the plate and the ground would be approximately 15 volts. Using these values for C_0 and R_1, and C_2 = 122 picofarads and $R_2 = 10^{14}$ ohms, the input impedance and cable capacitance values, we can solve equation (7).

Figure 3 shows the response as a function of displacement for fixed values of initial capacitance and Figure 4 shows the voltage response as a function of initial capacitance for given values of displacement. Examination of these figures shows that the output falls off almost linearly

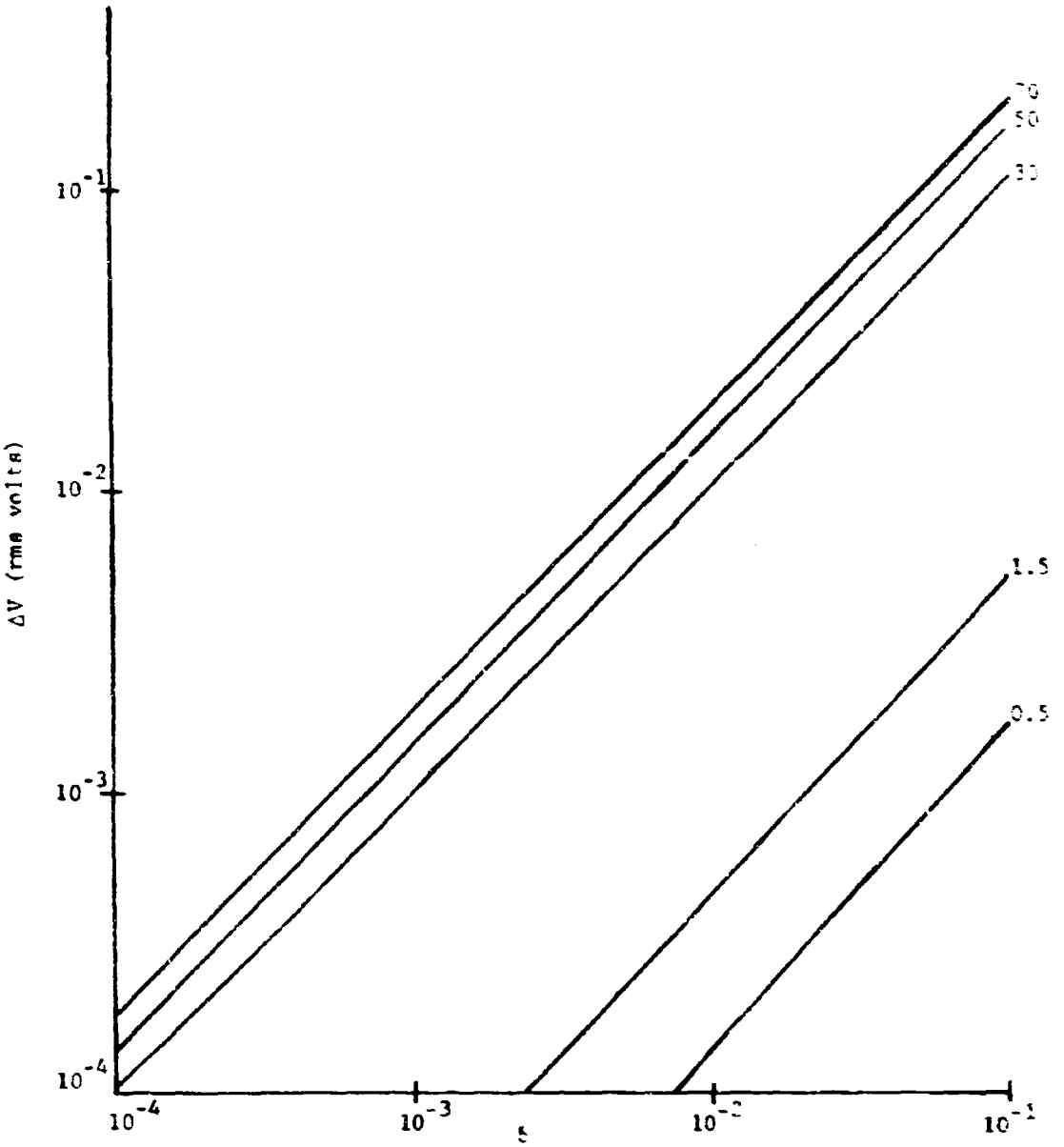

Figure 3. Probe Response as Function of Displacement, δ, for Given Values of Initial Capacitance (picofarads)

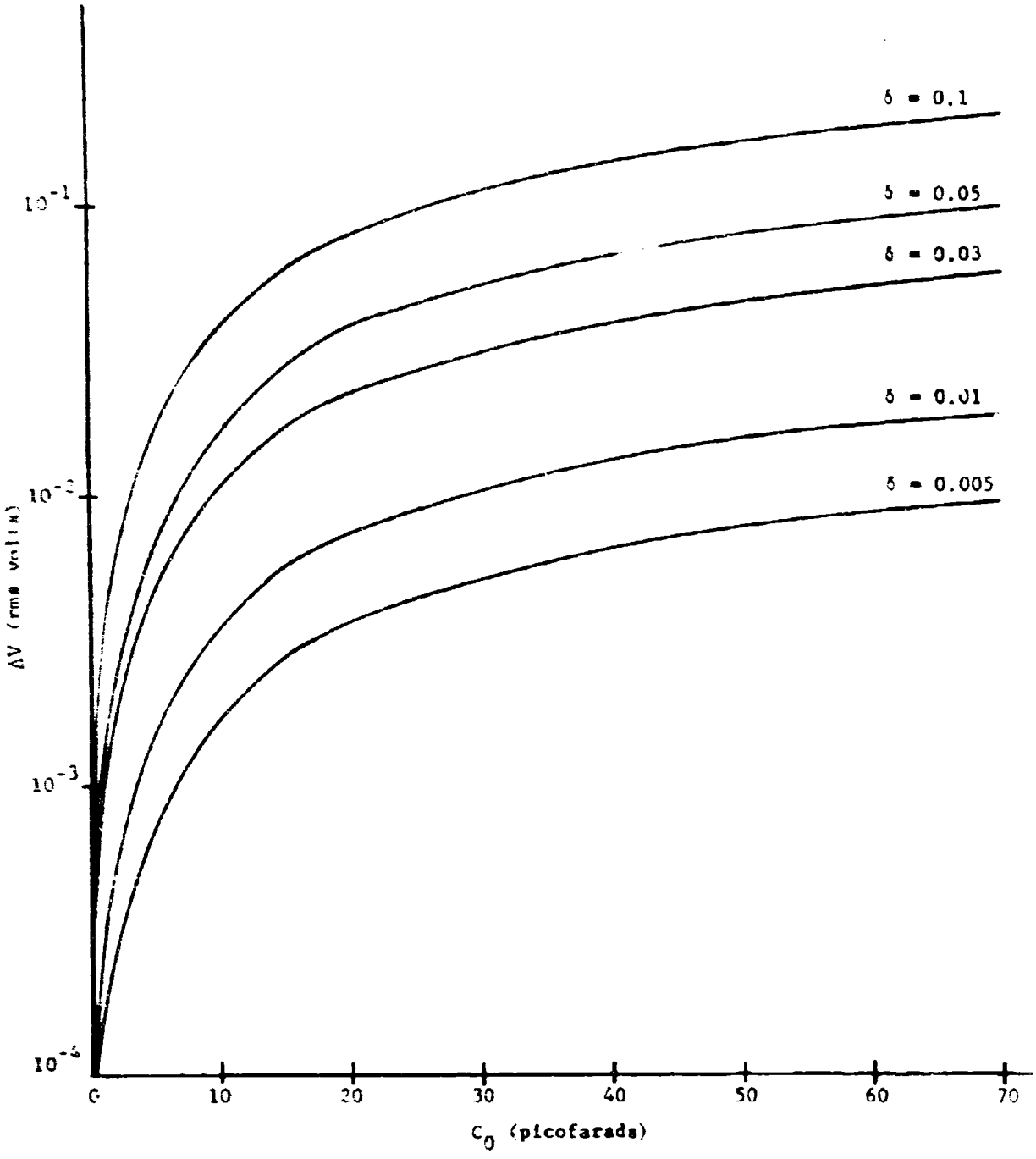

Figure 4. Probe Response as Function of Initial Capacitance for Given Values of Displacement

with displacement and is a linear function of capacitance for mid-values, while it is a higher order function at the extremes. We can see from Figure 3 that, for displacements on the order of a few thousandths of a percent of the probe-to-surface spacing, the voltage change is going to be in the microvolt region.

This model can be further refined by having only a portion of the bottom plate vibrate. This resembles the real world case more than the previous model where the whole bottom plate vibrated.

Figure 5(a) shows the geometry of the capacitor with part of the bottom plate at maximum displacement. This configuration can be transformed to the normal parallel plate capacitor shown in Figure 5(b) through the use of a Schwarz-Christoffel transformation (see Appendix A). Using this transformation assumes that the plates are infinite planes. However, if the spacing between the plates is small compared to the width of the plates, then the solutions obtained are good approximations of the finite case. We can extend our approximation to the case shown in Figure 5(c) by taking a truncated mirror image of Figure 5(a) and adding it to the original capacitor. This will be valid so long as h is small compared to d.

Transforming a stepped-capacitor to the w-plane and solving for the capacitance, we find that the increase in capacitance is slightly more than that obtained from two parallel capacitors, one at the wide spacing and one at the narrow spacing. This is expected because the transformation takes the internal fringing into account which is neglected when we consider the stepped capacitor as two parallel ones. If we further consider the stepped-capacitor shown in Figure 5(c) as the cross section of three disks instead of infinite planes, the error in capacitance value is greater due to the

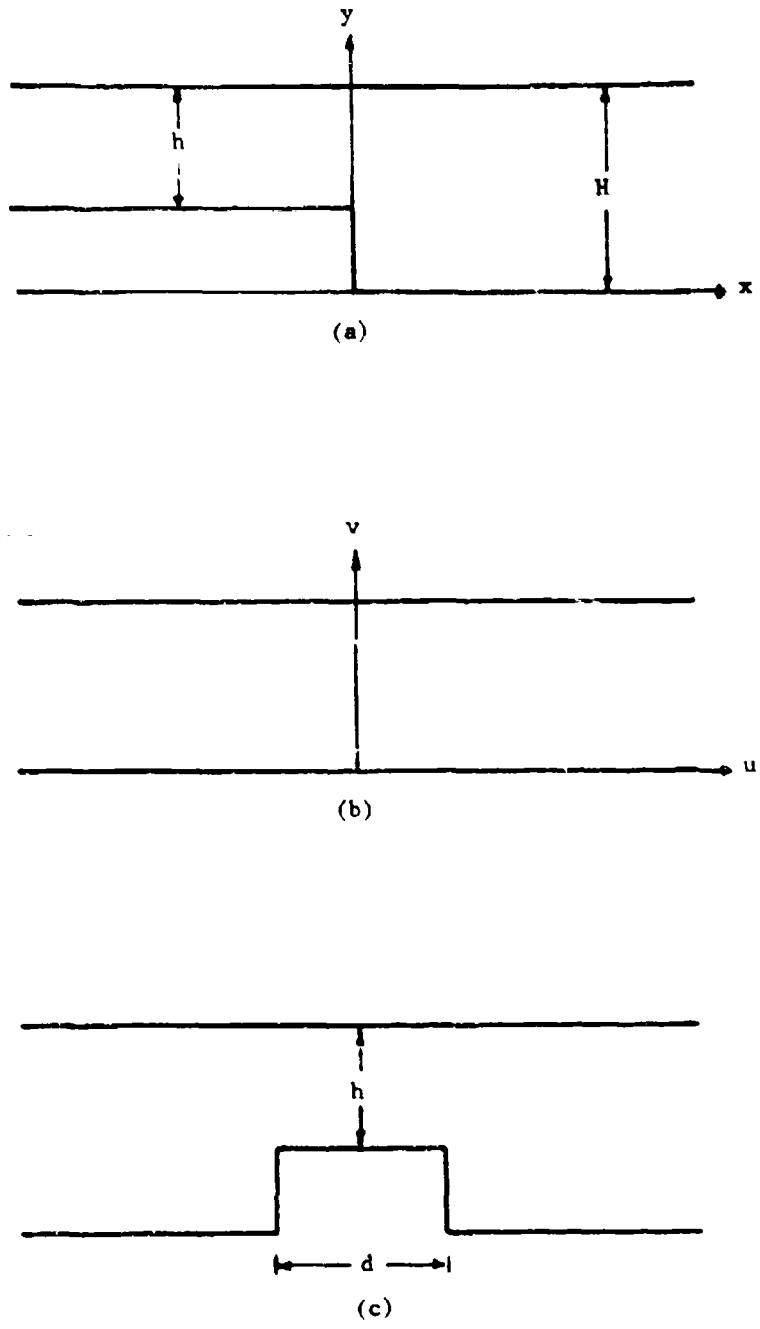

Figure 5. Geometry for Small Perturbation below Probe

increased amount of fringing that is being neglected. However, considering the capacitor as a fixed one and a smaller variable one will give us an order of magnitude results.

For example, assume we have a one-meter diameter probe at a height of 15 centimeters above the surface; the capacitance of this probe will be approximately 50 picofarads. If the area of perturbation has a radius of 5 centimeters and a peak-to-peak displacement of 1.5 millimeters, this will give us an initial capacitance of approximately 0.5 picofarads with δ equal to 0.01. Referring to either Figure 3 or 4 with these values we find that the voltage perturbation will be on the order of 10^{-4} volts.

A laboratory model of the parallel plate vibrating capacitor was constructed to test the validity of the measurement procedure. The model consisted of two parallel plates 6 inches in diameter connected to a voltage source through a resistor. The bottom plate was attached to a cam and driven by a motor at a 30 Hz vibration frequency. The experimental results for large values of δ agreed with the theoretical value of within 10-20% and to within 10% for small values of δ. Most of this error was attributed to mechanical instability of the model and qualitative experiments were run to prove that the varying component of the voltage was in fact caused by the varying capacitance and not by any outside influences.

III. NOISE ESTIMATES

A. Background

In Section II-A we showed how a surface disturbance could cause the potential at some point above it to vary. We further described a system to measure these disturbances. As in all physical systems, there are exogenous factors that enter the picture as noise or unwanted influences. The factors to be considered in this system are man-made electrical noise, such as 60 Hz noise, and random fluctuations in the local earth's electric field.

Using Maxwell's equations and assuming that the electric field is static and vertical and depends only on altitude, we know that

$$\frac{d\bar{E}}{dz} = \frac{\rho}{\epsilon_o}$$

$$\bar{J} = \sigma\bar{E}$$

and

$$\frac{d\bar{J}}{dz} = 0 \quad ;$$

therefore

$$\bar{J} = \bar{J}_o = \text{constant}$$

where ρ is the charge density, ϵ_o the free space permittivity, σ the conductivity, $\bar{E}$ the electric field strength, and $\bar{J}$ the current density. It can be shown that, subject to the boundary conditions

$$z \to \infty \ , \quad V \to 0,$$

the potential at the surface of the earth is

$$V(0) = \frac{\sigma_o q}{\epsilon_o} R$$

where q is the charge on the earth and R is the total resistance of the atmosphere. This equation has the form

$$V = IR$$

where

$$I = \frac{\sigma_o q}{\epsilon_o}$$

Variations in this current can be caused by changes in the conductivity or the surface charge density. The conductivity varies with the amount of pollution in the air and with changes in ionization levels due to increased cosmic ray penetration, point discharges, and lightning flashes. The surface charge density can vary locally with changing upper atmosphere charge conditions such as cloud passage and precipitation.

In order to examine the noise mechanism, the simplified model used the signal analysis has to be expanded. From the above model we can see that the current source is connected to the probe through a parallel resistor-capacitor network. The expanded model is shown in Figure 6. This model fits the actual atmospheric situation quite well. Suppose the lower atmosphere is in a quasi-static state and a fresh charge cloud suddenly appears. This will immediately produce a potential gradient at the ground (or any other reference point), calculable purely electrostatically. But, also immediately, the current flow will be altered, charges will move and a new quasi-static state

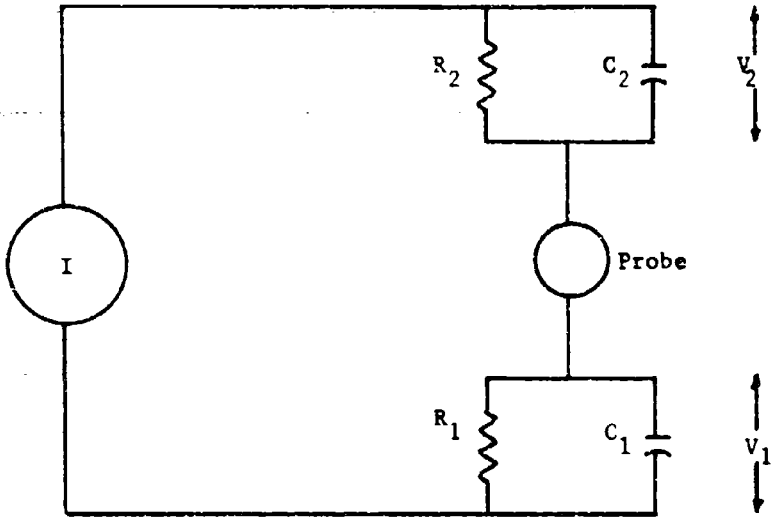

Figure 6. Expanded Probe Model

will be set up. This situation can be illustrated using Figure 6. The change in charge, Δq, causes a corresponding change in voltage, ΔV_1 and ΔV_2, across the capacitors. Since these are parallel RC circuits, the voltages across them at any time, t, due to this disturbance are equal to

$$V_1'(t) = \Delta V_1 \; e^{-t/R_1C_1}$$

$$V_2'(t) = \Delta V_2 \; e^{-t/R_2C_2}$$

The change in charge also changes the value of the current. This produces a voltage equal to

$$V_1''(t) = \Delta IR_1(1 - e^{-t/R_1C_1})$$

$$V_2''(t) = \Delta IR_2(1 - e^{-t/R_2C_2})$$

Therefore the voltage at the probe at any given time is the sum of these or

$$V_p(t) = V_1'(t) + V_1''(t)$$

$$V_p(t) = \Delta V_1 \; e^{-t/R_1C_1} + \Delta IR_1(1 - e^{-t/R_1C_1})$$

If there is a change of conductivity rather than of charge, then there is no electrostatic effect and

$$V_p(t) = \Delta I R_1 (1 - e^{-t/R_1 C_1})$$

Further examination of this model shows that the probe potential follows that of the surrounding atmosphere quite rapidly. If we take the special case where the conductivity is constant (i.e., no space charge distribution), this circuit acts as a simple resistive divider network since $R_1C_1 = R_2C_2$. Furthermore, if the probe is a thin disk parallel to the earth's surface, then the field distortion due to it will be confined to the immediate proximity of the probe. We can then consider the upper charge layer to lie on any undisturbed equipotential line close to the probe. This being the case, even with conductivity varying with height, it is readily apparent that, with all the changes assumed to be voltage changes occurring at some undisturbed equipotential line close to the probe, the probe will immediately respond.

B. Experiment Design

To measure and record the background fluctuations in the vertical component of the earth's electric field, a probe consisting of a one-meter diameter plate was mounted 15 centimeters above a ground plane approximately four meters square. The plate diameter and spacing were selected to provide a capacitance of approximately 50 picofarads and an equivalent leakage impedance of approximately 10^{12} ohms. With this leakage impedance, the input impedance of the electrometer ($\approx 10^{14}$ ohms) is large compared to the leakage impedance and thus the effect of the electrometer may be neglected.

Figure 7 shows a pictorial diagram of this. In this drawing, C_0 represents the capacitance between the probe and ground, C_1 represents the input capacitance

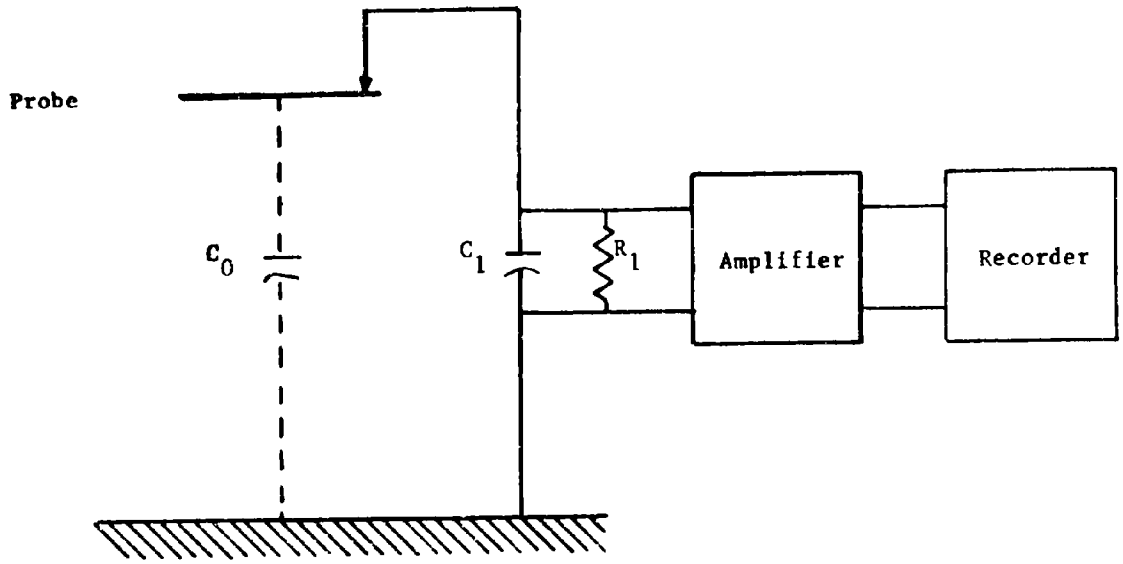

Figure 7. Pictorial Diagram of Experiment

of the electrometer and the capacitance of the cables connecting the probe to the electrometer, and R_1 represents the input resistance of the electrometer.

Several schemes were investigated for coupling the electrometer to the probe. The method which proved most successful used a triaxial cable made from a length of low loss coaxial cable with an additional outer shield. The inner shield was used as a guard in conjunction with a feedback circuit to reduce the effect of the cable capacitance. The circuit used with the electrometer is shown in Figure 8. As can be seen, an output signal from the electrometer proportional to the voltage between the center conductor and guard is amplified in the operational amplifier and fed back to the guard, thus reducing the difference in potential between the center conductor to a level determined by the gain of electrometer and the operational amplifier circuitry. This difference in potential, with the equipment used in this experiment, was a maximum of 30 millivolts with the center conductor (which is connected to the probe) at 120 volts above ground. Since the difference in potential between the center conductor and guard is small compared to the difference in potential between the central conductor and ground, we can measure the potential difference between the guard and ground and use this as an approximation to the actual potential difference on the probe with an error of less than 0.03%. In addition, the low output impedance (current source) characteristics of the operational amplifier make it useful for driving the recording instruments. An analysis of the gain of the electrometer-feedback circuit is included in Appendix B. An important

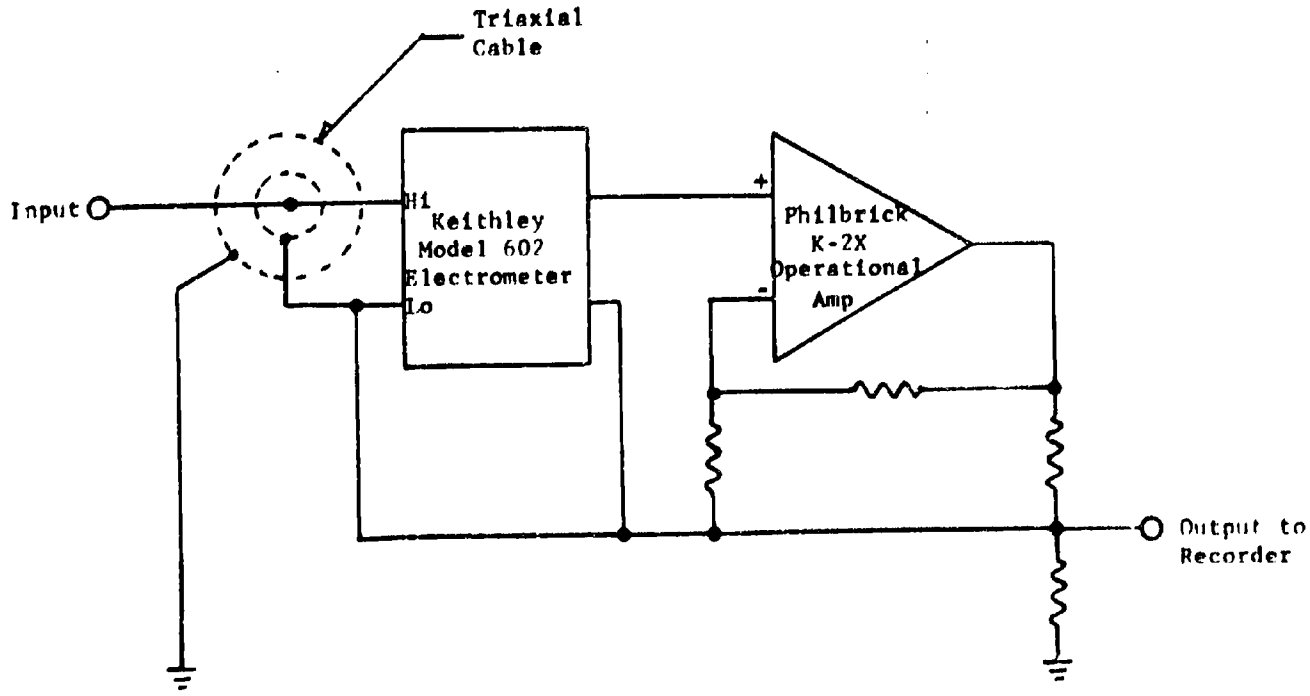

Figure 8. Electrometer Feedback Circuit

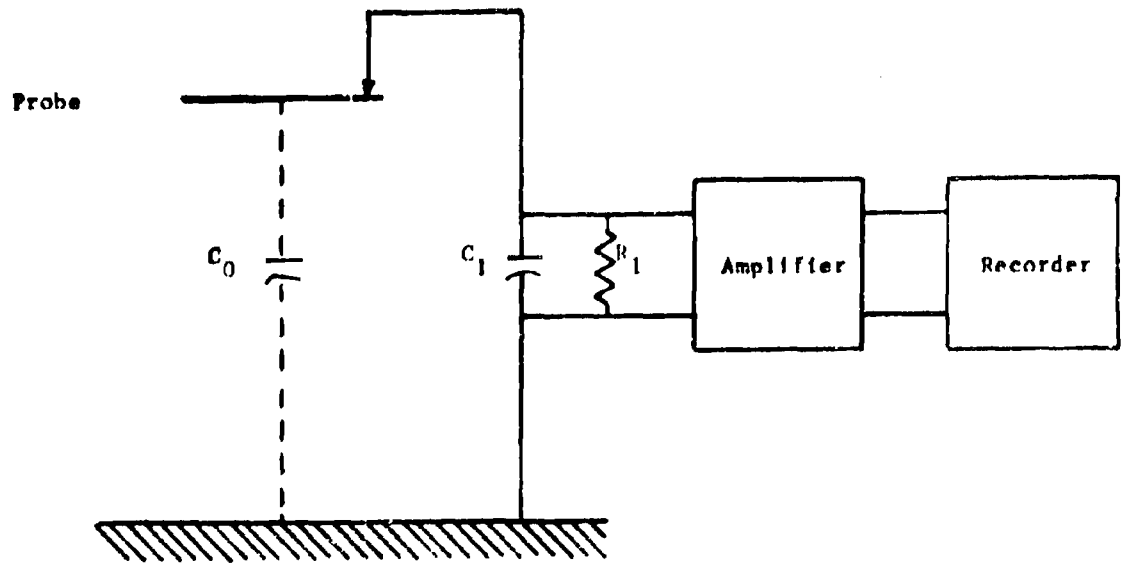

Figure 7. Pictorial Diagram of Experiment

feature of the feedback circuit is the reduction of the effective capacitance of the cable. As is shown in the analysis in Appendix C, the effective capacitance is reduced by approximately the gain of the electrometer-feedback circuitry. The effective input capactiance of the electrometer and cable to small signal changes is approximately 0.5 picofarad which is two orders of magnitude less than the capacitance of the probe, and therefore has an inconsequential effect on the measurements.

The frequency response of the probe can be determined by referring back to the model in Figure 6. For time variations slow compared to the time constant of the atmosphere, the transfer function for this circuit will be essentially that of a resistive voltage divider and is frequency independent. For time variations on the order of the relaxation time, the transfer function will be that of the series parallel RC circuit and a strong function of frequency. In the third regime, however, time variations are much faster than the atmospheric time constant; thus the capacitive reactance will be small compared to the resistive component. The circuit will behave as a capacitive voltage divider, and the transfer function will again be essentially independent of frequency. Thus, if frequencies much greater than the reciprocal of the atmospheric relaxation time are of interest, no consideration need be made of the frequency response of the probe. The primary considerations in probe design are that the input impedance of the electrometer be high compared to the leakage resistance at the probe and that the ratio of probe capacitance to miscellaneous stray capacitance (such as cable capacitance) be made large as feasible. This is due to the fact that cable capacitance increases the apparent size of the probe-to-ground capacitance without allowing

additional coupling to the atmospheric electric field which reduces the usable sensitivity of the probe to variations in the atmospheric electric field.

In order to obtain the dynamic range needed to display the whole spectrum from 0 to 100 Hz, some signal pre-conditioning was needed. This was accomplished through the use of filters and amplifiers to selectively amplify portions of the spectrum. Active filters of two types were constructed. One, a six pole Butterworth low pass with a 100 Hertz break frequency was used to band limit the data for purposes of eliminating aliasing in the analysis program. A second filter was constructed, a 0.01 Hertz six pole active Chebyshev highpass, and followed by an amplifier stage having a 10 dB gain. In recording the data, two channels on the recorder were used; one channel recorded the low-passed data, while the low-passed data passed through the 0.01 Hertz high pass filter and amplifier was recorded on another channel. Data records of thirty minutes to two hours' duration were made. After recording, the data was converted to digital form on a Radiation Analog-to-Digital Converter. The equivalent sampling rate used in A/D conversion was 1000 samples/second, thus insuring that all signal components to 100 Hz were recovered unambiguously. After the A/D operation, the digitized data was spectrally analyzed by Fast Fourier Transform techniques.

Figure 9 shows some typical results obtained from these measurements. These were obtained on a clear day with a slight wind. Figure 10 shows some results obtained when there was thunderstorm activity in the vicinity, the sky was cloudy and there was a slight wind. These results are somewhat typical

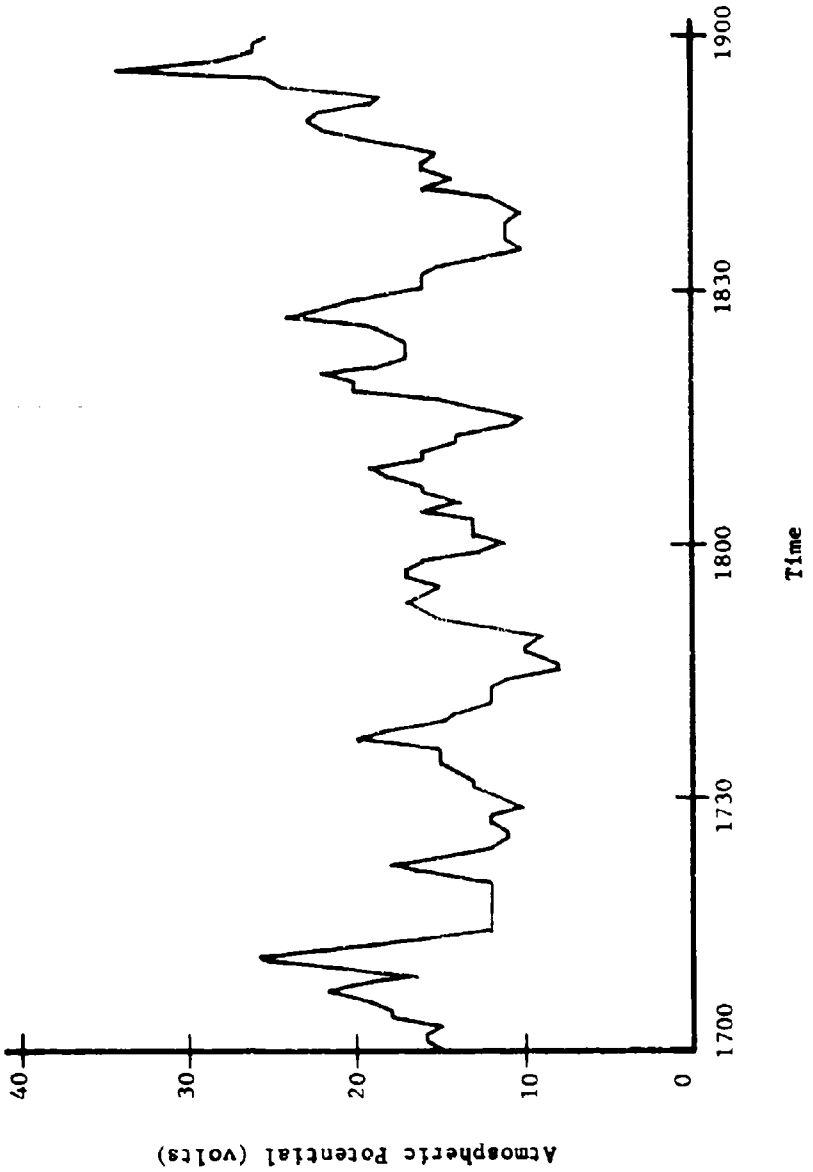

Figure 9. Atmospheric Potential Fluctuations as Measured by 1 Meter Diameter Probe 15 cm above Ground Plane—Fair Weather

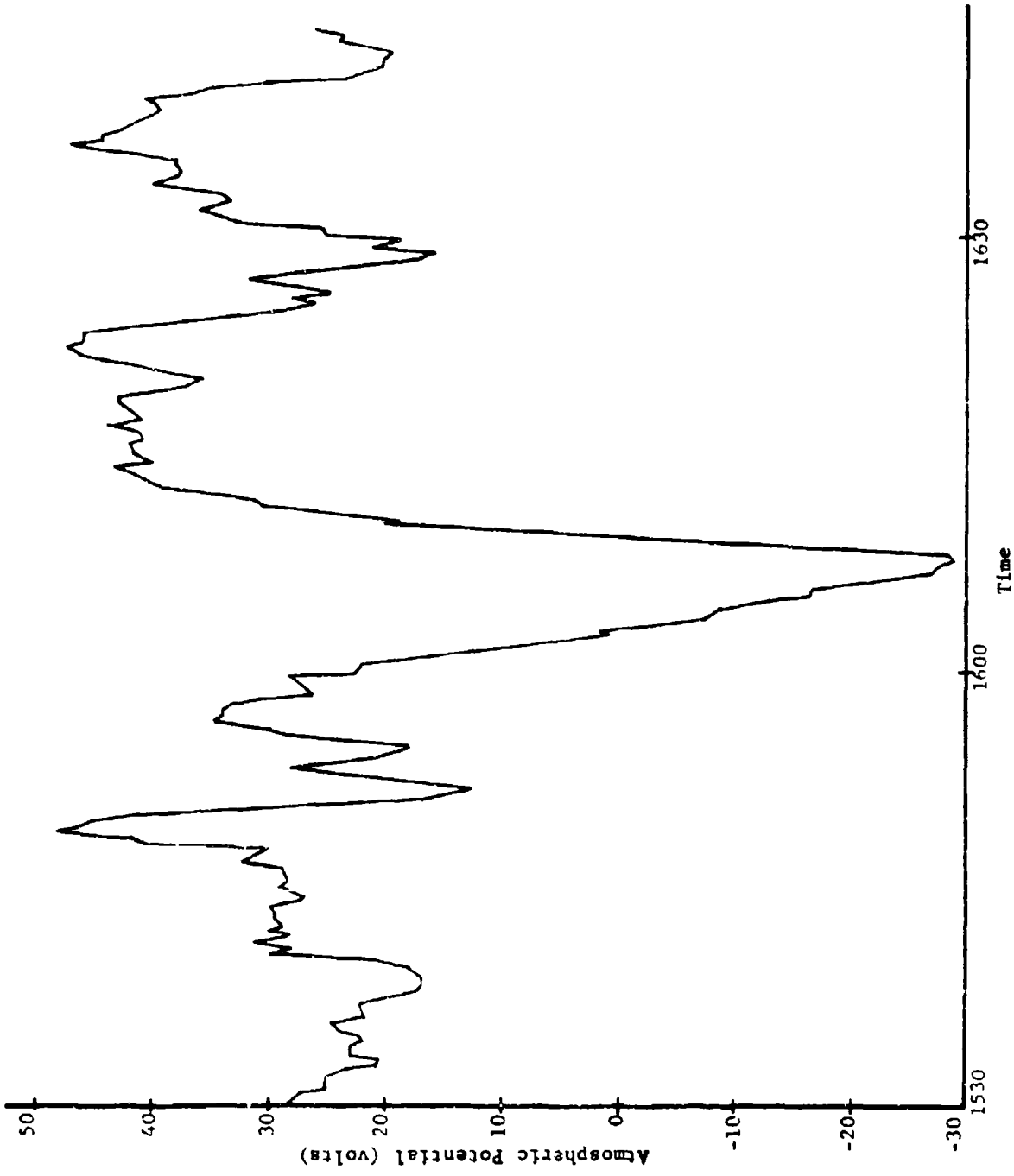

Figure 10. Atmospheric Potential Fluctuations as Measured by 1 Meter Diameter Probe 15 cm above Ground Plane—Thunderstorm Activity

and appear to agree with other published records,[1,2,3] and are shown principally to demonstrate that the system is capable of following rapid changes and is stable during slow variations.

C. Experimental Results

There are several options available for analysis of the data. One is to calculate the spectrum via the correlation function of the data; a second way is to directly transform the data. With either of these two approaches, weighting functions (lag windows and data windows) can be used to modify the data.

The first method above is the classical method of computing power spectra. One of the reasons for its widespread use was its computational economy. It took markedly fewer operations to calculate perhaps a tenth as many mean lagged products as there were data points and to Fourier transform the results than it did to calculate all the Fourier coefficients. The advent of the Fast Fourier Transform (FFT) has changed that—it is now faster to calculate all the Fourier coefficients. The former method is still highly popular, however, because it is so well established and most detailed practical problems encountered have accepted solutions available.

When all the Fourier coefficients are calculated, it would appear that the best approach would be to calculate the raw periodogram. This is basically a good approach, particularly if we have a periodic signal. However, with noise type signals, the leakage involved with the finite Fourier transform is too high. The best way to attack this problem is through the use of

windows. The choice of a window depends on the bandwidth of the effective filter and the statistical stability desired in the estimate. In other words, we are concerned with the trade-off between leakage and frequency resolution. The raw periodogram gives the best resolution and the worst leakage. Window functions reduce the leakage but at the expense of resolution. This is due to the fact that multiplying the data by a data window is equivalent to spectral averaging in the frequency domain. The mean square error is reduced but the spectral estimate is smeared out.

Several window functions were considered and tested. One of the easiest to use, and also one of the most popular, is cosine bell data window or Hann window. This corresponds to a three point smoothing with the points weighted 1/4, 1/2, 1/4. The effective bandwidth of the Hann window is twice that of the raw periodogram and the leakage is considerably reduced due to the reduction of the side lobes.

Another popular window function is the Hamming window. This corresponds to three point smoothing with weights 0.23, 0.54, 0.23. The bandwidth is just about the same as the Hann window, the first side lobe is lower but the height of the side lobes do not drop as fast as they do with the Hann window.

A third window function is the Parzen window. The bandwidth of this function is about 25% greater than that of the Hann or Hamming windows and the side lobes are substantially reduced. Because the main lobe is wider, the variability of the corresponding spectral estimates is less. Since the use of window functions is equivalent to smoothing the frequency

domain data, five point smoothing with equal weights was also used in the analysis. The equivalent bandwidth in this case is five times that of the raw periodogram; this reduces the variability of the spectral estimates considerably. One measure of this variability is the mean square error and it was calculated for each of the windows and found to be:

ϵ (raw periodogram) = 1.0
ϵ (Hann window) = 0.707
ϵ (Hamming window) = 0.707
ϵ (5 pt. smoothing) = 0.447
ϵ (Parzen) = 0.577

The information of most interest to this study was the rate of roll off of the spectrum. Therefore, statistical variability of the estimates was of greater importance than the resolution bandwidth. For this reason, the Parzen window and the five point smoothing appeared to be the best candidates for window functions. The data was analyzed using these window functions and the spectra obtained were virtually identical. An atmospheric noise spectrum obtained from these measurements is shown in Figure 11. The system noise was also measured and anlyzed and its spectrum is shown in Figure 12. The system noise data were obtained with the probe connected but electrostatically shielded from the earth's electric field.

The atmospheric noise spectrum falls off at a rate of 27 dB per decade from 0.2 Hz to 100 Hz. The spectrum level remains above that of the system noise from 0.1 Hz to about 50 Hz where it becomes noise limited. The major problem seems to be the dynamic range available on the tape recorder and could be overcome by further selective filtering and amplifying of the data. These

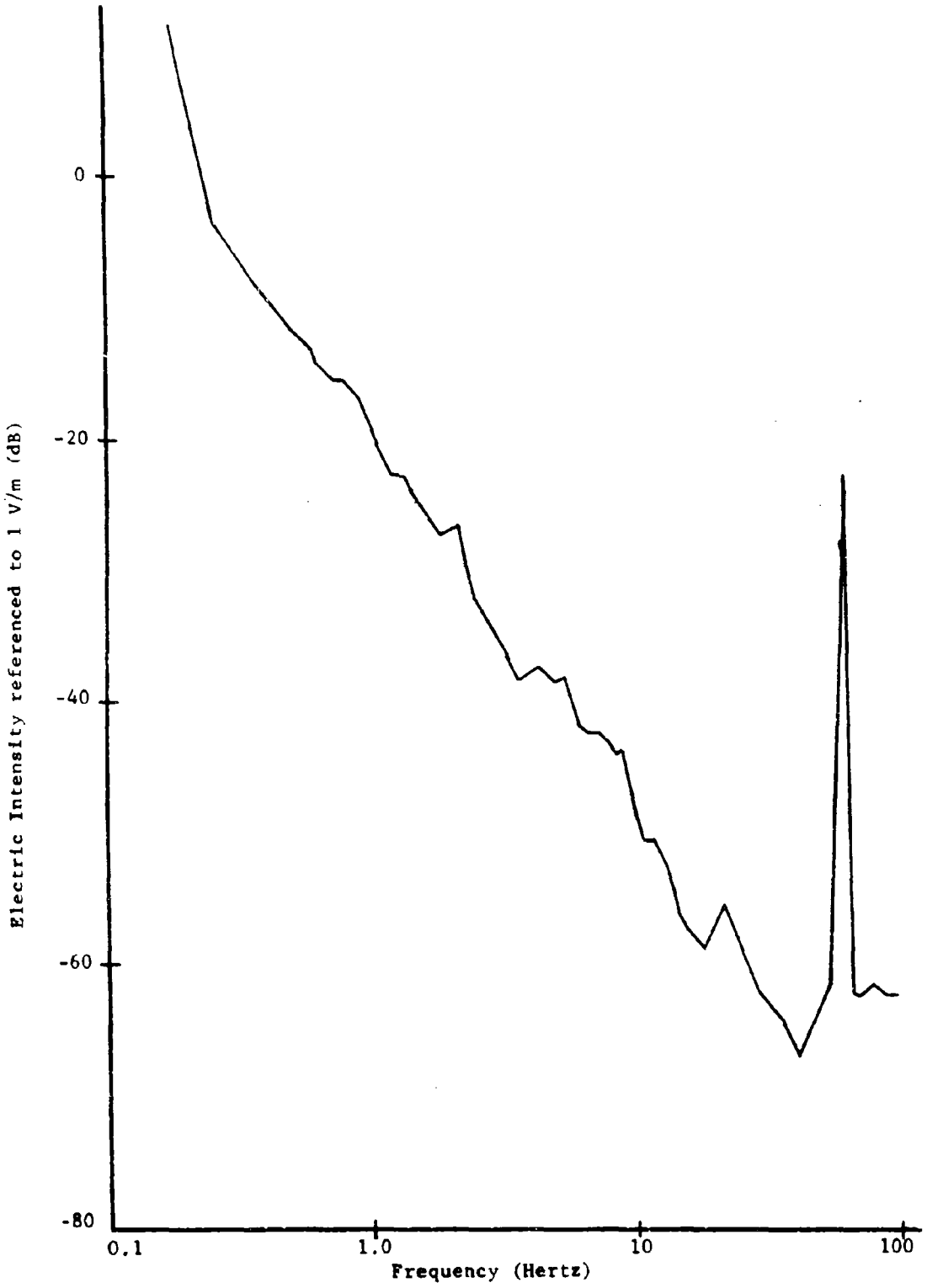

Figure 11. Atmospheric Noise Spectrum from 0.1 to 100 Hertz

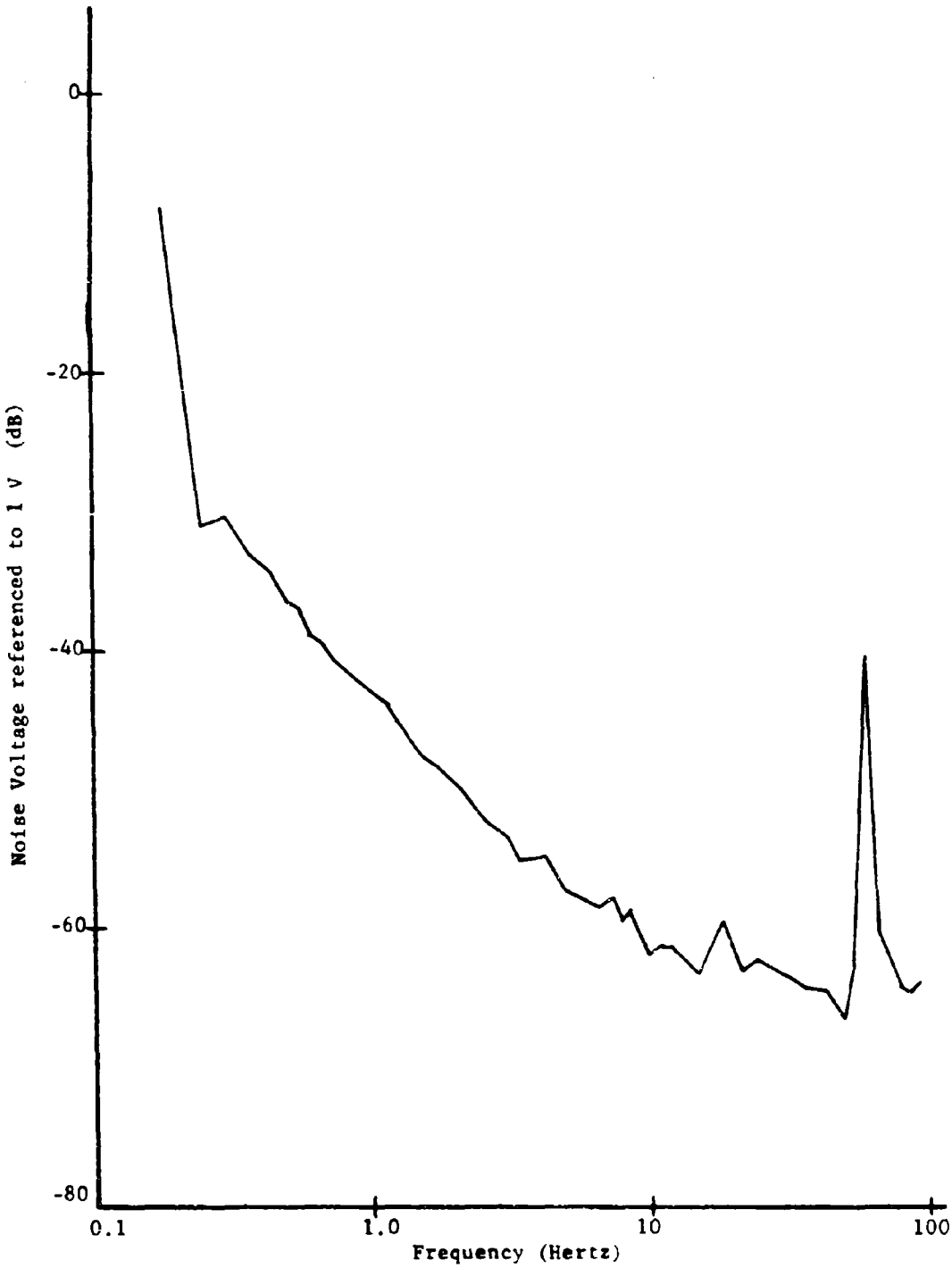

Figure 12. System Noise Spectrum from 0.1 to 100 Hertz

results are adequate to complete the analysis of the proposed surface perturbation measurement system and match favorably with those obtained at higher frequencies by E. L. Maxwell.[4] His results show the field intensity to be 70 dB below 1 volt/meter at 100 Hz and falling off at about 20 dB per decade above that point.

IV. ANALYSIS AND CONCLUSIONS

The signal estimates and the noise estimates can now be compared and some conclusions reached about the feasibility of using a suspended probe to measure surface perturbations. A suitable configuration for this analysis will be the same as that used for the noise measurements. This, it will be remembered, consisted of a 1 meter diameter plate suspended 15 centimeters above the ground, and the capacitance between the plate and ground was 50 picofarads. It was shown in Section I that, with this arrangement, a perturbation with about a 5 centimeter radius and a peak-to-peak displacement of 1.5 millimeters would cause a voltage perturbation on the order of 10^{-4} volts. Referring to the noise spectrum, we see that at 10 Hz the noise field intensity is about 40 dB below 1 volt/meter; this yields a noise voltage across the 15 centimeter gap of about 10^{-3} volts.

With this highly optimistic situation, the signal-to-noise ratio is less than 1. When the degrading effects of the real world are taken into account in the signal estimates, the ratio will be even worse. Also, most practical situations would require that the probe be suspended 1 meter or more above the ground. This would reduce the capacitance in the above example by a factor of 7 and would reduce the voltage perturbation by two orders of magnitude. The effect is compounded because the noise voltage is increased by a factor of about 7. We now have a signal level of about 10^{-6} volts and a noise level of about 10^{-2} volts. Some relief can be obtained by going to a higher frequency, but this does not give enough because the noise is reduced by only an order of magnitude per decade; most signals of interest would be below 1000 Hz.

V. REFERENCES

1. J. A. Chalmers, Atmospheric Electricity, Pergamon Press, New York (1967), p. 40.

2. B. F. J. Schonland, Atmospheric Electricity, John Wiley and Sons, Inc., New York (1953), p. 19.

3. W. D. Crozier, "Measuring Atmospheric Potential with Passive Antennas," Journal of Geophysical Research, Vol. 68, No. 18, September 15, 1963, p. 5173-79.

4. E. L. Maxwell, "Atmospheric Noise from 20 Hz to 30 kHz," Radio Science, Vol. 2, No. 6, June 1967, p. 637-644.

Appendix A

The Schwarz-Christoffel transformation allows the mapping of fields with polygonal boundaries in the z-plane into homogeneous fields with parallel boundaries in the w-plane. In most cases this cannot be accomplished in a single step, and it is first necessary to map the z-plane on an auxiliary t-plane such that the boundaries of the z-plane go over into the real axis of the t-plane. The t-plane is then transformed to the w-plane.

The problem is to map the polygonal boundary of the z-plane on the real axis of the t-plane, and then to map the parallel strip of the w-plane on the t-plane. Then integration constants have to be selected in such a fashion as to bring about a direct correspondence between these two mappings. If we let $(t - r_k) = \rho_k e^{i\theta_k}$ where the r_k are fixed points on the real axis of the t-plane, the real axis of the t-plane will transform into a polygon on the z-plane since

$$\frac{dz}{dt} = A(t - r_1)^{-\alpha_1} (t - r_2)^{-\alpha_2} \ldots$$

does not change directions except at the singular points r_k, and then it changes through an angle $\alpha_k \pi$. Expressed in integral form this mapping function is

$$A = A_1 \int \frac{dt}{(t - a_1)^{\alpha_1} (t - a_2)^{\alpha_2} \ldots} + A_2$$

Similarly, the t-plane can be mapped on the w-plane by

$$w = B_1 \int \frac{dt}{(t - r_1)^{\beta_1} (t - r_2)^{\beta_2} \ldots} + B_2$$

Figure A-1 shows the boundaries in the z-, t-, and w-planes; the Roman numerals indicate the points where two sides of the polygon meet. The unclosed portions are assumed to close at infinity and are indicated by dotted paths. The points II and III are arbitrarily located in the t-plane at 0 and +1 respectively. The parallel boundaries in the w-plane are taken to be equipotential surfaces with v = 0 and v = V. Setting up the differential equations

$$\frac{dz}{dt} = \frac{A_1}{(t - 0)^1 (t - 1)^{-\frac{1}{2}} (t - a)^{\frac{1}{2}}}$$

$$z = \int \frac{A_1}{t} \sqrt{\frac{t - 1}{t - a}}\, dt + A_2$$

$$= A_1 \left\{ \frac{1}{\sqrt{a}} \log \frac{\sqrt{a(t - 1)} - \sqrt{t - a}}{\sqrt{a(t - 1)} + \sqrt{t - a}} - \log \frac{\sqrt{t - 1} - \sqrt{t - a}}{\sqrt{t - 1} + \sqrt{t - a}} \right\} + A_2$$

$$\frac{dw}{dt} = \frac{B_1}{(t - 0)^1 (t - 1)^0 (t - \varepsilon)^0}$$

$$w = \int \frac{B_1}{t}\, dt = B_1 \log t + B_2$$

Integrating over paths I to determine A_1 and B_1

$$\int_{-\infty + j0}^{-\infty - jH} dz = \int_{\infty}^{-\infty} \frac{A_1}{t} \sqrt{\frac{t - 1}{t - a}}\, dt = \int_0^{\pi} A_1 \sqrt{\frac{R\, e^{j\theta} - 1}{R\, e^{j\theta} - a}}\, j d\theta$$

Therefore, $- jH = jA_1\pi$ for $R \to \infty$

$$A_1 = -H/\pi$$

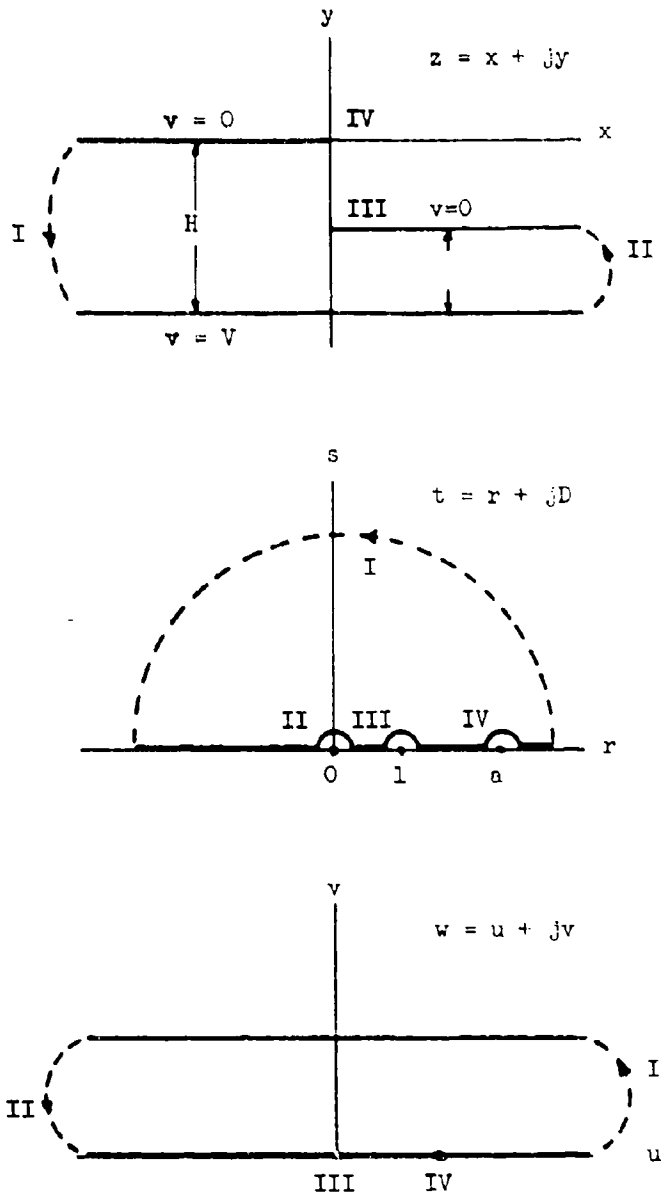

Figure A-1. Transformation Geometry

$$\int_{\infty + j0}^{\infty + jV} dw = \int_{\infty}^{-\infty} \frac{B_1}{t}\, dt = \int_0^{\pi} \frac{B_1 jR\, e^{j\theta}}{R\, e^{j\theta}}\, d\theta$$

Therefore, $jV = jB_1\pi$

$$B_1 = V/\pi$$

Integrating over path II

$$\int_{-\infty - jH}^{\infty + j(h - H)} dz = \int_{\pi}^{0} A_1 \sqrt{\frac{r\, e^{j\theta} - 1}{r\, e^{j\theta} - a}}\; jd\theta$$

Therefore, $jh = -j \frac{A_1}{\sqrt{a}}\pi$ for $r \to 0$

$$a = (H/h)^2$$

Comparison at point IV, $t = a$, $z = 0$, gives

$$z_{IV} = 0 = -\frac{H}{\pi}\left[\frac{h}{H}\log(1) - \log(1)\right] + A_2$$

Therefore, $A_2 = 0$

Comparison at point III, $t = +1$, $w = 0$, gives

$$w_{III} = 0 = \frac{V}{\pi}\log(1) + B_2$$

Therefore, $B_2 = 0$

Therefore,

$$w = \frac{V}{\pi}\log t$$

or

$$t = e^{(w\pi/V)}$$

Upon substitution of the integration constants

$$a = -\frac{H}{\pi}\left\{\frac{h}{H}\log\frac{H\sqrt{t-1} - h\sqrt{t-a}}{H\sqrt{t-1} + h\sqrt{t-a}} - \log\frac{\sqrt{t-1} - \sqrt{t-a}}{\sqrt{t-1} + \sqrt{t-a}}\right\}$$

APPENDIX B

The actual feedback circuit is constructed around a Philbrick K2-XA vacuum tube operational amplifier. The circuit may be analyzed as shown below.

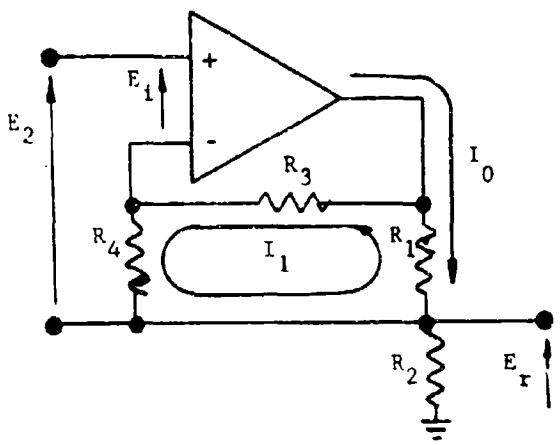

$$E_2 = E_i + I_1 R_4 \tag{1}$$

and

$$E_r = I_0 R_2 \tag{2}$$

Around the loop composed of R_1, R_3, and R_4

$$0 = I_1 R_3 + I_1 R_4 + (I_1 - I_0) R_1 \tag{3}$$

But for an ideal operational amplifier, $E_i \rightarrow 0$

Therefore,

$$R_4 I_1 = E_2 \qquad \text{or} \qquad I_1 = \frac{E_2}{R_4} \tag{4}$$

Substituting back into (4)

$$I_0 = -\frac{E_2}{R_1}\left(\frac{R_3 - R_1}{R_4} + 1\right) \tag{5}$$

Thus

$$G = \frac{E_R}{E_2} = -\frac{R_2}{R_1}\left(\frac{R_3 - R_1}{R_4} + 1\right) \tag{6}$$

The output of the feedback circuit is feedback along the low side of the electrometer input to form a guard or equipotential surface at the same (or nearly the same) potential as the high side of electrometer input, thus reducing the equivalent input capacitance. The output of the feedback circuit is also used to drive the recording instruments. Recordings are made of the output voltage on a standard pen chart recorder and through a low pass filter on magnetic tape. The magnetic tape is converted to digital form and the spectra computed using Fast Fourier Transform techniques.

APPENDIX C

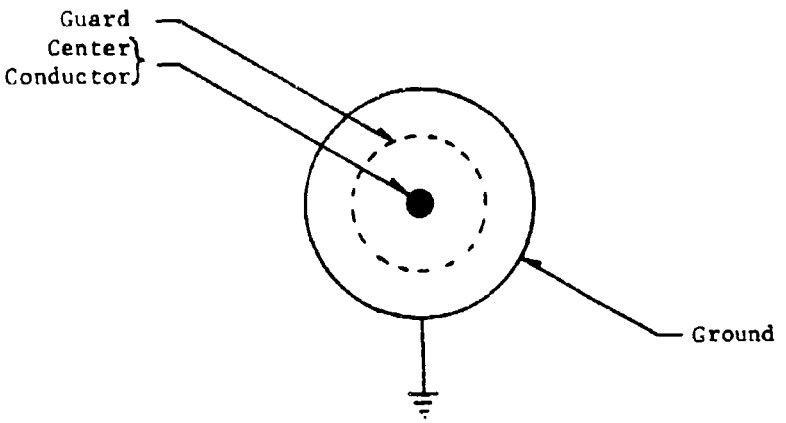

Capacitance of cable = C_0 center to guard

V_1 = Voltage from center conductor to ground

V_2 = Voltage from center conductor to guard

V_3 = Voltage from guard to ground

$$\left.\begin{aligned} V_2 + V_3 &= V_1 \\ V_3 &= GV_2 \\ V_2 + GV_2 &= V_1 \\ V_2 &= \frac{V_1}{1 + G} \end{aligned}\right\} \text{from Circuit Analysis}$$

If we understand quasi-static to mean that there are to be negligible currents flowing from the probe to the measuring instrument; or, in other words, the input impedance of our voltmeter is much greater than the leakage resistance to the atmosphere of the probe. The voltage to charge relationship on the cable will then be defined by

$$C_0 = \frac{q}{V_1}$$

where C_0 represents the shunt capacitance of the cable.

Further, if we let the input voltage change by an increment, ΔV_1, then an increment of charge, Δq_1, must be supplied to the shunt capacitance such that

$$\Delta q = C_0 \Delta V_1$$

If, however, we use a guarded cable such that the voltage from center conductor to guard is now V_2 such that

$$V_2 = \frac{V_1}{1 + G}$$

where

G = gain of feedback circuit

then

$$\Delta V_2 = \frac{\Delta V_1}{1 + G}$$

and

$$\Delta q' = C_0 \Delta V_2 = C_0 \frac{\Delta V_1}{1 + G}$$

or

$$\Delta q' = \frac{C_0}{1 + G} \Delta V_1$$

Thus, viewed from the input to the cable (the probe) by using a guarded cable in which the guard is maintained at nearly the same potential (with respect to ground) as the center conductor, we can reduce the effect of the capacitance of the cable.

Unclassified

Security Classification

DOCUMENT CONTROL DATA - R&D

(Security classification of title, body of abstract and indexing annotation must be entered when the overall report is classified)

1 ORIGINATING ACTIVITY (Corporate author)
Georgia Institute of Technology
Atlanta, Georgia 30332

2a REPORT SECURITY CLASSIFICATION
Unclassified

2b GROUP

3 REPORT TITLE

INVESTIGATION OF MANMADE AND NATURAL PERTURBATIONS OF THE EARTH'S SCIENTIFIC FIELD

4 DESCRIPTIVE NOTES (Type of report and inclusive dates)
Technical Report No. 6

5 AUTHOR(S) (Last name, first name, initial)

Bonham, C. H. III; and Langley, J. B.

6 REPORT DATE
30 October 1970

7a TOTAL NO OF PAGES
45

7b NO OF REFS
4

8a CONTRACT OR GRANT NO.
Nonr-991(08)

b. PROJECT NO.

c.

d

9a ORIGINATOR'S REPORT NUMBER(S)
Technical Report No. 6
A-519

9b OTHER REPORT NO(S) (Any other numbers that may be assigned this report)

10 AVAILABILITY/LIMITATION NOTICES

11 SUPPLEMENTARY NOTES

12 SPONSORING MILITARY ACTIVITY
Office of Naval Research
Department of the Navy
Arlington, Virginia 22217

13 ABSTRACT

This report describes an investigation of the effect of low frequency periodic perturbations of the height of a conducting surface on the earth's local electric field.

Simulation of small, low audio frequency vibrations of a portion of a conducting surface indicate that such displacement will result in perturbations to the normal component of the electric field above that surface. The exact magnitude of these perturbations is a function of the type of probe used to sense the perturbations and the probe-to-surface distance and is, in general, on the order of microvolts.

Atmospheric noise spectra were obtained by use of a passive antenna measurement scheme. The data obtained were analyzed using the Fast Fourier Transform and noise spectra on the band 0.1 to 100 Hertz were acquired. The noise spectra thus obtained indicate that atmospheric noise appears to fall off at the rate of 27 dB per decade in the region 0.1 to 100 Hertz.

Examination of the signal-to-noise ratios implies that the performance of this system in detection of sea surface vibrations would be marginal at best.

DD FORM 1 JAN 64 1473

Unclassified

Security Classification

Unclassified

Security Classification

14 KEY WORDS	LINK A ROLE	LINK A WT	LINK B ROLE	LINK B WT	LINK C ROLE	LINK C WT
Conductivity Analyses Acoustic Perturbations Electromagnetic-Acoustic Interactions						

INSTRUCTIONS

1. ORIGINATING ACTIVITY: Enter the name and address of the contractor, subcontractor, grantee, Department of Defense activity or other organization (*corporate author*) issuing the report.

2a. REPORT SECURITY CLASSIFICATION: Enter the overall security classification of the report. Indicate whether "Restricted Data" is included. Marking is to be in accordance with appropriate security regulations.

2b. GROUP: Automatic downgrading is specified in DoD Directive 5200.10 and Armed Forces Industrial Manual. Enter the group number. Also when applicable, show that optional markings have been used for Group 3 and Group 4 as authorized.

3. REPORT TITLE: Enter the complete report title in all capital letters. Titles in all cases should be unclassified. If a meaningful title cannot be selected without classification, show title classification in all capitals in parenthesis immediately following the title.

4. DESCRIPTIVE NOTES: If appropriate, enter the type of report, e.g., interim, progress, summary, annual, or final. Give the inclusive dates when a specific reporting period is covered.

5. AUTHOR(S): Enter the name(s) of author(s) as shown on or in the report. Enter last name, first name, middle initial. If military, show rank and branch of service. The name of the principal author is an absolute minimum requirement.

6. REPORT DATE: Enter the date of the report as day, month, year, or month, year. If more than one date appears on the report, use date of publication.

7a. TOTAL NUMBER OF PAGES: The total page count should follow normal pagination procedures, i.e., enter the number of pages containing information.

7b. NUMBER OF REFERENCES: Enter the total number of references cited in the report.

8a. CONTRACT OR GRANT NUMBER: If appropriate, enter the applicable number of the contract or grant under which the report was written.

8b, 8c, & 8d. PROJECT NUMBER: Enter the appropriate military department identification, such as project number, subproject number, system numbers, task number, etc.

9a. ORIGINATOR'S REPORT NUMBER(S): Enter the official report number by which the document will be identified and controlled by the originating activity. This number must be unique to this report.

9b. OTHER REPORT NUMBER(S): If the report has been assigned any other report numbers (*either by the originator or by the sponsor*), also enter this number(s).

10. AVAILABILITY/LIMITATION NOTICES: Enter any limitations on further dissemination of the report, other than those imposed by security classification, using standard statements such as:

(1) "Qualified requesters may obtain copies of this report from DDC."

(2) "Foreign announcement and dissemination of this report by DDC is not authorized."

(3) "U. S. Government agencies may obtain copies of this report directly from DDC. Other qualified DDC users shall request through _____."

(4) "U. S. military agencies may obtain copies of this report directly from DDC. Other qualified users shall request through _____."

(5) "All distribution of this report is controlled. Qualified DDC users shall request through _____."

If the report has been furnished to the Office of Technical Services, Department of Commerce, for sale to the public, indicate this fact and enter the price, if known.

11. SUPPLEMENTARY NOTES: Use for additional explanatory notes.

12. SPONSORING MILITARY ACTIVITY: Enter the name of the departmental project office or laboratory sponsoring (*paying for*) the research and development. Include address.

13. ABSTRACT: Enter an abstract giving a brief and factual summary of the document indicative of the report, even though it may also appear elsewhere in the body of the technical report. If additional space is required, a continuation sheet shall be attached.

It is highly desirable that the abstract of classified reports be unclassified. Each paragraph of the abstract shall end with an indication of the military security classification of the information in the paragraph, represented as *(TS)*, *(S)*, *(C)*, or *(U)*.

There is no limitation on the length of the abstract. However, the suggested length is from 150 to 225 words.

14. KEY WORDS: Key words are technically meaningful terms or short phrases that characterize a report and may be used as index entries for cataloging the report. Key words must be selected so that no security classification is required. Identifiers, such as equipment model designation, trade name, military project code name, geographic location, may be used as key words but will be followed by an indication of technical context. The assignment of Links, rules, and weights is optional.

DD FORM 1473 (BACK)

Unclassified

Security Classification